This article has been accepted for publication in a future issue of this journal, but has not been fully edited. Content may change prior to final publication. Citation information: DOI 10.1109/TIE.2018.2842735, IEEE Transactions on Industrial Electronics

Long-range Fast Nanopositioner Using Nonlinearities of Hybrid Reluctance Actuator for Energy Efficiency

Shingo Ito, Stefan Troppmair, Bernhard Lindner, Francesco Cigarini, and Georg Schitter, *Senior Member*

***Abstract*—While nanopositioners often use flexures for high quality motion avoiding nonlinearities, the achievable motion range and energy efficiency are limited due to the force required for positioning against the flexures. To overcome the problem, this paper proposes a flexure-guided nanopositioner with a nonlinear hybrid reluctance actuator for a large range and energy efficiency. The actuator has nonlinear negative stiffness that partially cancels the flexures' stiffness. Consequently, the nonlinearities reduce the required current by up to 67 %. To compensate them for high-precision motion in the entire range of 2 mm, a feedback controller is designed, achieving a closed-loop bandwidth of 640 Hz and positioning resolution of 2.48 nm(RMS). The mechatronic system is designed such that the flexure nonlinearity has no influence on the closed-loop stability and bandwidth. Additionally for accurate periodic scanning motion, modeling-free inversion-based iterative control is combined to decrease the tracking error by a factor of 396 at most. The achieved error is 10 nm(RMS) for a 1 Hz triangular motion of 1.6 mm range and for a 100 Hz triangular motion of 10 μm range. The results demonstrate that the proposed nanopositioner can play a role of both long-stroke and high-speed scanners with the improved power consumption.**

***Index Terms*—Actuators, motion control, nanopositioning, magnetic circuits.**

I. Introduction

FOR manufacturing and inspection with nanometer resolution, such as 3D printing [1] and atomic force microscopy (AFM) [2] in a production line [3], compact nanopositioners are indispensable to carry and scan the materials and the samples. To improve the productivity of the manufacturing and inspection systems, the nanopositioners need to realize fast motion with nanometer resolution over a long range. For the compactness and linearity, these nanopositioners usually have a mover that is guided by flexures and actuated by high-precision actuators [4].

Piezoelectric actuators are used for their high force, small size and extremely high bandwidth [5], [6]. Because the achievable control bandwidth is typically up to the first dominant resonant frequency [7], it is increased with the high stiffness of the piezoelectric materials and the flexures [8]. In return, the achievable range is strictly limited for a given actuation force, resulting in a strict trade-off between the bandwidth and range. Furthermore, piezoelectric actuators have nonlinearities such as hysteresis to be compensated for precise motion [9].

Lorentz actuators (e.g. voice coil actuators) utilize the Lorentz force, which is independent of the mover position with a uniform flux density for high linearity [10], and the flexures dominate the stiffness between the mover and the stator. Furthermore, these actuators enable a closed-loop bandwidth significantly higher than the first resonant frequency by design [11]. Thus, the stiffness can be lowered to some extent by the flexure design for large motion [12] and high disturbance rejection [13]. However, low-stiffness flexures can create anti-resonances and resonances at low frequencies [14], which may demand a higher current for actuation and may restrict the bandwidth, respectively. Similarly, resonances to restrict the bandwidth occur at low frequencies when negative-stiffness flexures are combined to cancel the guiding flexures' stiffness, as simulated by finite element analysis (FEA) in [15]. A disadvantage of Lorentz actuators is their relatively small motor constant (i.e. force-to-current ratio), which can restrict the force and the range [10]. The motor constant can decrease around the stroke ends due to the fringing of the magnetic flux [10]. These properties are undesired also for fast motion requiring a high acceleration force.

To overcome the above limitations, a high-speed actuator may be combined with a long-range actuator as a dual stage actuator (DSA) [16], [17]. However, a second actuator complicates the system and control design [18]. Furthermore, the high-speed actuator may generate the reaction force that excites the long-range actuator, dependent on the configuration. The compensation of the problematic force requires an additional actuator [19], balance mass [20] or heavy long-range actuator [21], which impairs the systems' compactness. Due to those disadvantages, a single actuator is rather desired particularly for motion within a few millimeters.

Manuscript received Month xx, 2xxx; revised Month xx, xxxx; accepted Month x, xxxx. The financial support by the Austrian Federal Ministry for Digital, Business and Enterprise, and the National Foundation for Research, Technology and Development, MICRO-EPSILON MESSTECHNIK GmbH & Co. KG and ATENSOR Engineering and Technology Systems GmbH is gratefully acknowledged.

S. Ito, F. Cigarini, and G. Schitter are with Christian Doppler Laboratory for Precision Engineering for Automated In-Line Metrology, Automation and Control Institute (ACIN), TU Wien, Vienna A-1040, Austria (e-mail: ito@acin.tuwien.ac.at).

S. Troppmair and B. Lindner are with the Automation and Control Institute (ACIN), TU Wien, Vienna A-1040, Austria.

Post-print version of the article: S. Ito, S. Troppmair, B. Lindner, F. Cigarini, and G. Schitter, "Long-Range Fast Nanopositioner Using Nonlinearities of Hybrid Reluctance Actuator for Energy Efficiency," *IEEE Transactions on Industrial Electronics*, vol. 66 (4), pp. 3051-3059, 2019. DOI: 10.1109/TIE.2018.2842735

This article has been accepted for publication in a future issue of this journal, but has not been fully edited. Content may change prior to final publication. Citation information: DOI 10.1109/TIE.2018.2842735, IEEE Transactions on Industrial Electronics

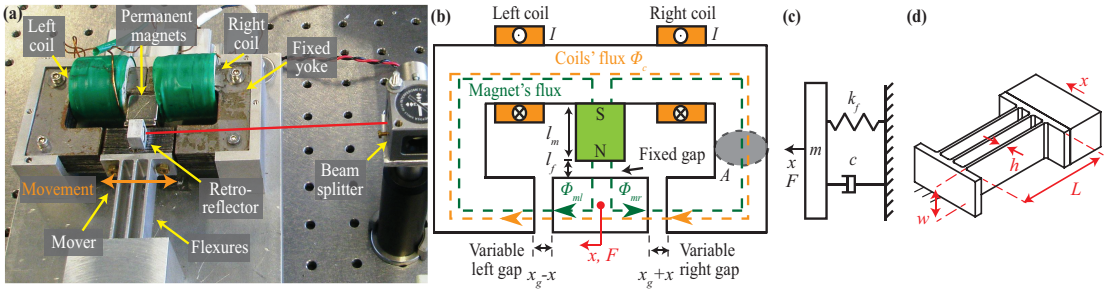

Fig. 1. Nanopositioner using hybrid reluctance actuator: (a) photograph, (b) illustration showing the actuation principle, (c) damped mass-spring system modeling the nanopositioner, and (d) 3D model of the flexures with their dimension.

Although nanopositioners are usually designed to be linear with flexures for high quality motion, their proportionality between the displacement and force fundamentally restricts the actuation range and energy efficiency. This is because large motion needs a sufficiently high force against the flexure force. In the meantime, control algorithms are developed to compensate for the residual nonlinearities of the nanopositioners (e.g. actuators' hysteresis), including sliding mode control [22], adaptive control [23] and iterative control [24].

To enable large motion with reduced power consumption, this paper proposes a nanopositioner that utilizes nonlinearities, which are integrated to be compensated by motion control relatively easily for high bandwidth and precision. The proposed nanopositioner is guided by flexures and equipped with a hybrid reluctance actuator. Hybrid reluctance actuators have a motor constant that is several times lager than a comparable Lorentz actuator [10] and have been applied to fast tool servos [25] and steering mirrors [26]. In this paper, the nonlinear negative stiffness of the hybrid reluctance actuator is used to partially cancel the flexures' stiffness. Consequently a small coil current is sufficient for large motion, improving the energy efficiency. This mechatronic system is designed for a closed-loop system with robust stability for high quality motion. Additionally, iterative control is used to accurately track a periodic trajectory to demonstrate achievable performance.

This paper is organized as follows. Section II introduces the proposed nanopositioner with the hybrid reluctance actuator, which is investigated in Section III. Section IV presents a measured frequency response for the verification and the feedback control design, which is discussed with iterative control design in Section V. Section VI presents experimental results. Section VII concludes the paper.

II. System description

Fig. 1(a)(b) shows the proposed nanopositioner with a hybrid reluctance actuator and its actuation principle. A small ferromagnetic yoke is laterally guided by flexures as the mover to achieve high acceleration. Among different types of flexures, leaf-spring flexures are selected and manufactured from aluminum for their capability to realize low stiffness and large motion [4]. The stator consists of a relatively large yoke, a Nd-Fe-B permanent magnet, and two identical coils.

TABLE I
Dimension of the developed nanopositioner

Dimension	Value	Description
x_g	1 mm	Left and right gaps at the origin
l_f	1 mm	Fixed gap
l_m	19 mm	Magnet length
A	15 mm × 15 mm	Cross-section area of the flux paths

The permanent magnet creates a biasing flux to be distributed to the left and right air gaps around the mover, as indicated by the green lines in Fig. 1(b). When a current is applied to the coils, an additional flux is created, as shown by the orange line. By superimposing these two types of flux, the force on a side of the mover is stronger than the other, creating a lateral actuation force F. The hybrid reluctance actuator is designed to provide a large actuation range of 2 mm, and its yokes are manufactured from laminated electrical steel sheets (EN10025-S235JR) to reduce the eddy current [27]. Table I lists the dimensions of the developed hybrid reluctance actuator, which is further discussed in Section III.

To provide the current, the coils are connected in series and driven by a custom-made current amplifier. It has a -3 dB bandwidth of 3.2 kHz, with a maximum output current and voltage of ±5 A and ±15 V, respectively. To measure the mover position, a cube-corner retroreflector (43-305, Edmund optics, Barrington, USA) is mounted on the mover, and an interferometer (10899A, Agilent Technologies, Santa Clara, USA) is used. The sensor has a resolution of 1.25 nm/bit. For high quality motion, control is implemented by the CPU (DS1005, dSpace GmbH, Paderborn, Germany) of a rapid prototyping control system at a sampling frequency of 20 kHz, using a 16-bit DAC (DS2102) and FPGA (DS5203) to interface it with the current amplifier and the interferometer, respectively.

III. System analysis

A. Hybrid reluctance actuator

To analyze the hybrid reluctance force, the flux in Fig. 1(b) is derived by assuming that the permeability of the yokes are sufficiently large [26]. The magnetic reluctances of the left

Post-print version of the article: S. Ito, S. Troppmair, B. Lindner, F. Cigarini, and G. Schitter, "Long-Range Fast Nanopositioner Using Nonlinearities of Hybrid Reluctance Actuator for Energy Efficiency," *IEEE Transactions on Industrial Electronics*, vol. 66 (4), pp. 3051-3059, 2019. DOI: 10.1109/TIE.2018.2842735

This article has been accepted for publication in a future issue of this journal, but has not been fully edited. Content may change prior to final publication. Citation information: DOI 10.1109/TIE.2018.2842735, IEEE Transactions on Industrial Electronics

gap R_l, the right gap R_r, the fixed gap R_f and the permanent magnet R_m are given by

$$R_l = \frac{x_g - x}{\mu_0 A},\ R_r = \frac{x_g + x}{\mu_0 A},\ R_f = \frac{l_f}{\mu_0 A},\ R_m = \frac{l_m}{\mu_0 A}, \quad (1)$$

where x is the mover position from the center, and x_g is the left and right air gaps at $x = 0$. While l_f, l_m and μ_0 are the fixed gap, the magnet length and the vacuum permeability, respectively, A is the cross-section area of the flux paths. By applying Hopkinson's law [10], the total flux given by the permanent magnet Φ_{mt} is

$$\Phi_{mt} = \frac{H_c l_m \lambda}{R_m + R_f + \frac{R_r R_l}{R_r + R_l}}, \quad (2)$$

where the coercive force H_c is about 1 MA/m. The coefficient λ is introduced to take account of the flux leakage [28] and the fringing flux [29]. Dependent on x, Φ_{mt} is separated into the flux through the left gap Φ_{ml} and through the right gap Φ_{mr}:

$$\Phi_{ml} = \Phi_{mt} R_r/(R_l + R_r),\ \Phi_{mr} = \Phi_{mt} R_l/(R_l + R_r). \quad (3)$$

Since the magnet is regarded as a long air gap in (1), the coils' flux Φ_c does not go through the magnet, resulting in

$$\Phi_c = 2NI/(R_l + R_r), \quad (4)$$

with the current I and winding number $N = 120$ of each coil.

By applying the Maxwell's stress tensor, the lateral force F of the hybrid reluctance actuator is derived as [26]

$$F = \frac{(\Phi_c + \Phi_{ml})^2 - (\Phi_c - \Phi_{mr})^2}{2\mu_0 A} = K_m(x)I + k_a(x)x, \quad (5)$$

where the motor constant K_m and the actuator stiffness k_a are given as follows, by assuming that l_m is sufficiently longer than l_f:

$$K_m(x) = \frac{2\mu_0 A N \lambda H_c l_m}{2 l_m x_g + x_g^2 - x^2}, k_a(x) = \frac{2\mu_0 A \lambda^2 H_c^2 l_m^2 x_g}{(2 l_m x_g + x_g^2 - x^2)^2}. \quad (6)$$

Note that the nonlinearity due to x^2 in the denominator of Eq. (6) occurs because x influences Φ_{mt} [26], [28].

While the above analytical model reveals a source of the actuator's nonlinearities, it is difficult to analytically determine the coefficient λ [10], which may depend on x. Therefore, FEA is used with a software (Maxwell, ANSYS, Canonsburg, USA) to compute K_m and k_a, as shown in Fig. 2(a). It is visible that they are small at the center ($x = 0$) and increase around the stroke ends ($x = \pm x_g$). In conventional hybrid-reluctance systems [26], [28], such nonlinearities are regarded as unwanted properties. However, the proposed nanopositioner utilizes them, as discussed in the next section.

B. Lumped mass model and current for actuation

To investigate the nonlinearities' influence, the nanopositioner is described by a lumped mass model in Fig. 1(c) with a mover mass m of 55 g. The damping c is usually way smaller than the critical damping. The flexures' stiffness k_f is related to their length L, width w and height h (Fig.1(d)) by [14]

$$k_f = nEwh^3/L^3, \quad (7)$$

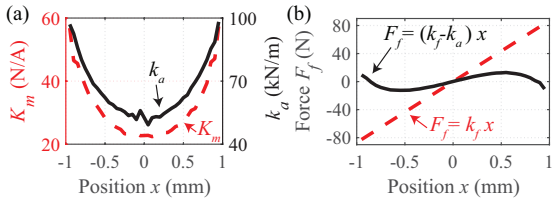

Fig. 2. Simulated parameters: (a) the motor constant K_m and the actuator stiffness k_a by FEA, and (b) the total stiffness force F_f with and without the actuator stiffness k_a.

with the Young's modulus $E = 72$ GPa. The number of the flexures $n = 3$ as well as $L = 40$ mm, $w = 15$ mm and $h = 1.2$ mm are determined by using modal analysis (Workbench, ANSYS) such that the rotational modes of the flexure-guided mover occur at a high frequency of 800 Hz or higher. This is highly desired for high closed-loop bandwidth and robust stability as discussed in Section V. The resulting k_f is 87 kN/m.

The equation of motion is related to (5)

$$F = K_m(x)I + k_a(x)x = m\ddot{x} + c\dot{x} + k_f x. \quad (8)$$

For a quasi-static response, it is rewritten as

$$I = \frac{F_f(x)}{K_m(x)} = \frac{k_f - k_a(x)}{K_m(x)}x, \quad (9)$$

where $F_f = (k_f - k_a)x$ is the total stiffness force that needs to be compensated for a displacement of x. Fig. 2(b) shows the simulated F_f with and without the actuator stiffness k_a. Without k_a, a displacement within a range of about ± 1 mm requires a force of more than ± 80 N against the flexure stiffness force $k_f x$. This high force is reduced to less than ± 15 N by combining it with k_a. This is because k_a partially cancels k_f in (9), which is more effective toward the stroke ends of ± 1 mm, as the negative value with k_a increases. In summary, this simulation clearly demonstrates that the proposed nanopositioner enables large motion with a small current and high energy efficiency.

C. Open-loop stability

Because the actuator stiffness k_a canceling the flexure stiffness k_f in (9) can cause a stability problem, its influence is investigated by linearizing (8) at an equilibrium point x_0, from which the transfer function $P(s)$ from the current to the mover position is derived as follows

$$P(s) = K_m(x_0)/(ms^2 + cs + k_l(x_0)), \quad (10)$$

using the linearized total stiffness k_l given by

$$k_l(x_0) = \left.\frac{\partial F_f(x)}{\partial x}\right|_{x=x_0} - \left(\left.\frac{\partial K_m(x)}{\partial x}\right|_{x=x_0}\right)\frac{F_f(x_0)}{K_m(x_0)}. \quad (11)$$

The poles p of the plant is derived from (10) as

$$p = \frac{-c \pm \sqrt{c^2 - 4mk_l(x_0)}}{2m}. \quad (12)$$

According to (11), k_l is larger than zero around the center of $x_0 = 0$, where F_f is zero and has positive slope in Fig. 2(b).

Post-print version of the article: S. Ito, S. Troppmair, B. Lindner, F. Cigarini, and G. Schitter, "Long-Range Fast Nanopositioner Using Nonlinearities of Hybrid Reluctance Actuator for Energy Efficiency," *IEEE Transactions on Industrial Electronics*, vol. 66 (4), pp. 3051-3059, 2019. DOI: 10.1109/TIE.2018.2842735

This article has been accepted for publication in a future issue of this journal, but has not been fully edited. Content may change prior to final publication. Citation information: DOI 10.1109/TIE.2018.2842735, IEEE Transactions on Industrial Electronics

In this case, the poles given by (12) are in the left-half of the Laplace transform s-plane. Consequently, stability of the nanopositioner is guaranteed around the center. This also allows to carry out system identification for control design. When the mover is far from the center, however, F_f can be non-zero with negative slope, resulting in negative k_l. In this case, the nanopositioner is unstable because a pole occurs in the right-half plane, which is compensated by feedback control in Section V.

IV. Frequency Response

As an experimental evaluation, a Bode plot from the current amplifier input to the mover position is measured when the measurement point x_0 is changed within 0 - 0.9 mm by superimposing an offset to the sine sweep input. When x_0 is set to zero, the frequency response is measured in an open loop for the feedback control design in Section V-A. For the other cases, the nanopositioner is stabilized by the resulting controller for evaluation. The results in Fig. 3 show the first resonant frequency at 178 Hz for $x_0 = 0$ mm, which gradually decreases as x_0 increases up to 0.6 mm. This is because the natural frequency $\omega_n = \sqrt{|k_l|/m}$ approximates the first resonant frequency, and k_l gradually decreases.

When x_0 is 0.8 mm and 0.9 mm, the resonance peak vanishes. This can be explained by replacing s by $j\omega$ in (10)

$$P(j\omega) = K_m(x_0)/(k_l(x_0) - \omega^2 m + j\omega c). \qquad (13)$$

When the nanopositioner is open-loop unstable due to the unstable pole, k_l is negative and does not cancel out $-\omega^2 m$ at ω_n in the denominator of Eq. (13), unlike the stable case. Consequently the magnitude shows well-damped low-pass characteristics. Overall, Fig. 3 demonstrates the open-loop stability of the nanopositioner around the center, validating the analysis in Section III-C.

Fig. 3 shows a phase lag at high frequencies due to the current amplifier's dynamics and due to the eddy current [27]. More importantly, the magnitude variation at the frequencies higher than 300 Hz is not as significant as the lower frequencies. This is because the stiffness does not influence the dynamics at the frequencies sufficiently higher than ω_n in (13), which are determined mainly by K_m and the the mass m. The -40 dB/dec mass line shows a slight variation dependent on x_0, which would be due to the variation of K_m. Notice that the second resonant frequency at 841 Hz is almost insensitive to x_0. Because such a mode can restrict the closed-loop bandwidth, this insensitivity is highly desired to decrease uncertainties for handling in the control design.

V. Motion Control

For experimental demonstrations, a triangular wave, commonly used as scanning motion in AFM [2], is selected as the motion trajectory r. To track it precisely, Fig. 4 shows the control of the nanopositioner with the stabilized system's reference u and the current amplifier's dynamics $P_a(s)$, which has low-pass characteristics. The control design and analysis are presented in this section.

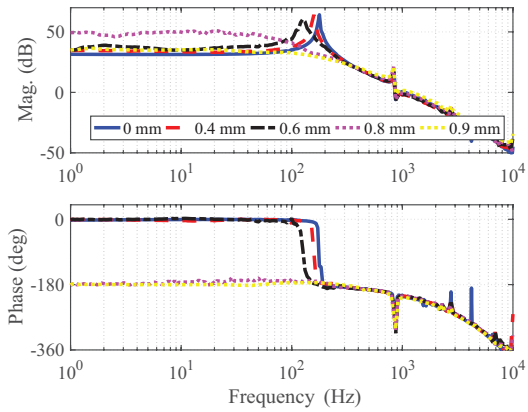

Fig. 3. Measured Bode plot from the current amplifier input to the position x. The measurement point x_0 is varied within 0 - 0.9 mm by superimposing a DC offset to the sine sweep input.

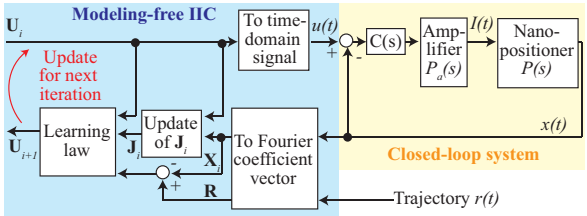

Fig. 4. Control architecture of the nanopositioner, where $C(s)$ denotes a feedback controller, and a modeling-free IIC is used to track a periodic trajectory r.

A. Feedback control design

To enable high-precision long-stroke motion, a feedback controller $C(s)$ is used to stabilize the nanopositioner, as shown in Fig. 4. To compensate for the second mechanical resonance that is almost insensitive to x_0 in Fig. 3, a notch filter is used as a part of $C(s)$. In addition, $C(s)$ includes a lead compensator providing a phase lead to set the open-loop cross-over frequency ω_c beyond 300 Hz for high bandwidth and robust stability. Finally a PI controller is combined to eliminate the steady-state error due to the static stiffness of the plant as follows (cf. [13])

$$C(s) = g_c \left(\frac{s + \frac{\omega_c}{10}}{s}\right)\left(\frac{3s + \omega_c}{s + 3\omega_c}\right)\left(\frac{s^2 + 0.1 d_N \omega_N s + \omega_N^2}{s^2 + 0.1\omega_N s + \omega_N^2}\right) \qquad (14)$$

where $\omega_N = 2\pi \times 841$ rad/s and $d_N = -15$ dB are the notch frequency and depth for the second resonance, respectively. The controller gain g_c is tuned to maximize ω_c with a sufficient phase margin of more than 30° for the measured response at 0 mm in Fig. 3. The resulting g_c and ω_c are -22 dB and 358 Hz, respectively.

B. Feedback control analysis and validation

For closed-loop stability analysis, Nyquist stability criterion [30] is applicable, and it can be simplified in a case of open-loop stable systems (the simplified Nyquist criterion [30]).

Post-print version of the article: S. Ito, S. Troppmair, B. Lindner, F. Cigarini, and G. Schitter, "Long-Range Fast Nanopositioner Using Nonlinearities of Hybrid Reluctance Actuator for Energy Efficiency," *IEEE Transactions on Industrial Electronics*, vol. 66 (4), pp. 3051-3059, 2019. DOI: 10.1109/TIE.2018.2842735

This article has been accepted for publication in a future issue of this journal, but has not been fully edited. Content may change prior to final publication. Citation information: DOI 10.1109/TIE.2018.2842735, IEEE Transactions on Industrial Electronics

In this section, Nyquist stability criterion is used when the nanopositioner is open-loop unstable at first.

When $P(s)$ has the unstable pole with negative k_l, the open-loop transfer function $C(s)P_a(s)P(s)$ at a sufficiently low frequency has high gain due to the integrator of $C(s)$ and phase approximating to

$$\lim_{\omega \to +0} \angle C(j\omega)P_a(j\omega)P(j\omega) = -90^\circ + 0^\circ - 180^\circ = -270^\circ. \tag{15}$$

Thus, the locus on a Nyquist diagram starts from the top along the imaginary axis and approaches the origin at high frequencies ($+\infty$) due to the strictly proper system, as shown by solid lines in Fig. 5(a). The plot also shows the locus mirrored about the real axis for the response from $\omega = -\infty$ to -0, and the +0 and -0 ends are connected by a clockwise semicircle (dashed lines), due to $C(s)$'s integrator [30]. For closed-loop stability, the connected solid and dashed lines must encircle the -1 point once in the counterclockwise direction because of the unstable pole, according to Nyquist stability criterion [30]. To satisfy this condition in Fig. 5(a), the -1 point must lie on the left side of the locus from $\omega = +0$ to $+\infty$, as the solid black line indicates. (Otherwise the system is unstable, without counterclockwise encirclement around the -1 point (the red lines).) This stability requirement is same as the simplified Nyquist criterion for open-loop stable systems. In other words, whether the pole is stable or unstable, a feedback controller including an integrator can stabilize a flexure-guided hybrid reluctance actuator by providing sufficient phase margin and gain margin, which are based on the simplified Nyquist criterion [30].

Fig. 5(b) shows a Nyquist diagram of the open-loop transfer function simulated with the measured response in Fig. 3. Regardless of the measurement position x_0, phase margin (PM) of more than 30° is ensured for robust stability. This is realized by the cross-over frequency ω_c sufficiently higher than the natural frequency ω_n, so that the stiffness variation does not influence the dynamics around ω_c (Fig. 3). In fact, ω_c is within 350±15 Hz for any x_0 in Fig. 5(b). Such control design is possible with the parasitic mechanical modes that are sufficiently higher than ω_n, as designed in Section III-B.

For validation, the complementary sensitivity function $T(s)$ from $u(t)$ to $x(t)$ in Fig. 4 is measured when the measurement point x_0 is changed within 0 - 0.9 mm by superimposing an offset to the sine sweep input. The results in Fig. 6 show a high closed-loop bandwidth (-3 dB) of at least 640 Hz even if x_0 varies. This successfully demonstrates that the careful mechatronic system design allows the same controller $C(s)$ to stabilize the nanopositioner whether it is open-loop stable or unstable. However, the Bode plot shows a magnitude variation up to about 10 dB dependent on x_0 beyond 20 Hz, where the gain of $C(s)$ is not large enough to completely compensate for the nanopositioner's nonlinearities. The residual nonlinearities are compensated for scanning by iterative control in the next section.

C. Iterative control

The residual nonlinearities observed in Fig. 6 is problematic to accurately track r. Additionally, dependent on the mover position, the open-loop transfer function has an integrator, and the nanopositioner becomes a Type 1 system [30], which tracks the ramp parts of the triangular trajectory r with an error. Although feedforward control may be used for compensation, an accurate model needs to be identified for the design [10], which can be time-consuming due to the nonlinearities. Therefore, for the proposed nanopositioner, modeling-free inversion-based iterative control (IIC) [24], [31], [32] is selected.

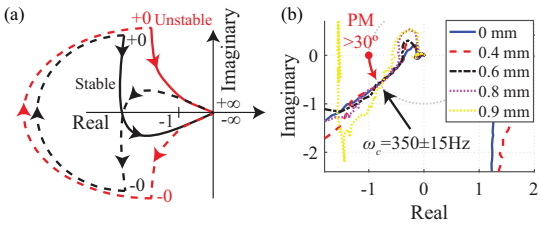

Fig. 5. Nyquist diagram of the open-loop transfer function $C(s)P_a(s)P(s)$: (a) conceptual plot when $P(s)$ has the unstable pole due to negative k_l, and (b) simulated plot for the positive frequencies that is based on the measured response in Fig. 3 at different measurement point x_0.

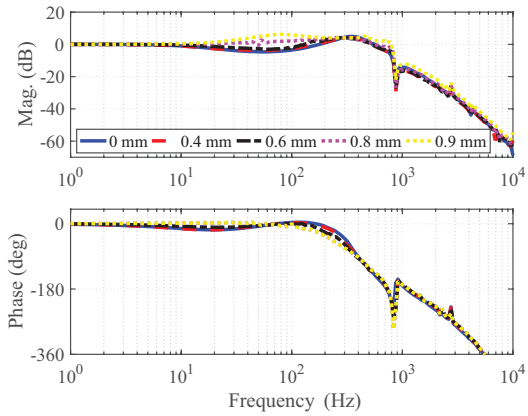

Fig. 6. Measured complementary sensitivity function $T(s)$ for the validation of $C(s)$. The measurement point x_0 is varied within 0 - 0.9 mm by superimposing a DC offset to the sine sweep input.

Modeling-free IIC learns from the previous trial to update the control input, significantly decreasing the tracking error. To take an advantage that the periodic trajectory r consists of fundamental and harmonic frequency components, modeling-free IIC can learn at those discrete frequencies only. This is beneficial to eliminate the measurement noise between the harmonic frequencies [32] and to reduce its algorithm and the required computation power [33]. Furthermore, modeling-free IIC performs system identification during learning, and its design requires no model in advance.

As shown in Fig. 4, modeling-free IIC is implemented in the frequency domain by Fourier coefficient vector $\mathbf{U}$, $\mathbf{X}$ and $\mathbf{R}$ for $u(t)$, $x(t)$ and $r(t)$, respectively [32]:

$$\mathbf{U} = [u_1 \ldots u_k \ldots u_q]^T, \quad \mathbf{X} = [x_1 \ldots x_k \ldots x_q]^T, \tag{16}$$

$$\mathbf{R} = [r_1 \ldots r_k \ldots r_q]^T, \quad \text{where } r_k = 0 \text{ for } k > q_r, \tag{17}$$

Post-print version of the article: S. Ito, S. Troppmair, B. Lindner, F. Cigarini, and G. Schitter, "Long-Range Fast Nanopositioner Using Nonlinearities of Hybrid Reluctance Actuator for Energy Efficiency," *IEEE Transactions on Industrial Electronics*, vol. 66 (4), pp. 3051-3059, 2019. DOI: 10.1109/TIE.2018.2842735

This article has been accepted for publication in a future issue of this journal, but has not been fully edited. Content may change prior to final publication. Citation information: DOI 10.1109/TIE.2018.2842735, IEEE Transactions on Industrial Electronics

where u_k, x_k and r_k are the k-th complex Fourier coefficients of the respective signals. While q is the highest harmonics compensated by modeling-free IIC to determine its bandwidth, q_r is the highest harmonics of the trajectory. Since the nanopositioner's nonlinearities deform the periodic motion and create higher harmonics, $q_r < q$ is desired. The learning law is [32]

$$\mathbf{U}_{i+1} = \mathbf{U}_i + \mathbf{J}_i^{-1}(\mathbf{R} - \mathbf{X}_i), \tag{18}$$

where i is the trial number, and $\mathbf{J}_i$ is a Jacobian matrix representing the plant.

For modeling-free IIC, $\mathbf{J}_i$ is identified and updated during learning, and the secant method [24], [31], [32] is used for fast and accurate learning. In this case, $\mathbf{J}_i$ is a diagonal matrix, and its k-th diagonal element is updated by

$$j_{k,i} = \begin{cases} \frac{x_{k,i} - x_{k,i-1}}{u_{k,i} - u_{k,i-1}} & \text{for } |u_{k,i} - u_{k,i-1}| \geq \epsilon, \\ j_{k,i-1} & \text{otherwise,} \end{cases} \tag{19}$$

where ϵ is a threshold for stable learning [32] and tuned to 10 pm at the implementation. As the initial condition, an identity matrix is used for $\mathbf{J}_{-1}$ with $\mathbf{U}_{-1} = \mathbf{X}_{-1} = 0$, resulting in $\mathbf{U}_0 = \mathbf{R}$. In other words, the nanopositioner at the 0th iteration is controlled only by feedback control. For the convergence of IIC, the convergence criteria [34] needs to be satisfied, and convergence properties of modeling-free IIC with the secant method are investigated in [31]. In this paper, the convergence and effectiveness of modeling-free IIC is experimentally evaluated for the nanopositioner using the hybrid reluctance actuator in Section VI-D.

VI. Experimental Results

A. Nominal parameter values

The motor constant K_m and the actuator stiffness k_a are evaluated at the center $x = 0$ as nominal performance by a force sensor (K6D27, ME-Messsysteme, Hennigsdorf, Germany). The sensor is connected to the mover, and the resulting force is measured when a current of ± 0.2 A is applied to the coils. From the result, 8.48 N/A is obtained as the nominal motor constant K_m. For the actuator stiffness, the force is measured at ± 0.1 mm without the current. As a result, the combined stiffness $k_f - k_a$ at the center is given by 57 kN/m. Since k_f given by (7) is 87 kN/m, k_a is estimated at 30 kN/m. Notice that the evaluated K_m and k_a are smaller than the FEA by a factor of 2.7 and 1.6, respectively. The difference would be due to the manufacturing and assembly tolerance.

B. Step response

The positioning resolution of the nanopositioner is evaluated at static points by measuring a response to 4 nm steps. For this evaluation, the nanopositioner is stabilized by the controller $C(s)$ without modeling-free IIC. Fig. 7 shows the reference u and measured position x. Although the nanopositioner is open-loop unstable at 0.8 mm, the error $u - x$ at this point shows a peak-to-peak value of ± 8 nm and an RMS value of 2.48 nm, validating the controller design enabling static positioning with nanometer resolution. Consequently, the 4 nm steps are clearly resolved in Fig. 7. Note that the RMS error is close to the resolution of the interferometer (1.25 nm).

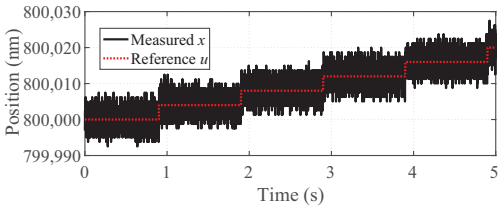

Fig. 7. Measured response to steps of 4 nm around the 800 μm point.

C. Slow ramp motion

To evaluate the current I in a quasi steady state (cf. Eq. (9)), a slow ramp of about 40 μm/s is used as the reference u for the closed-loop system without modeling-free IIC. During the experiment, the voltage over the coils is measured by a probe (N2791A, Keysight, Santa Rosa, USA) and the coil current is calculated from the amplifier input, from which the power consumption of the nanopositioner is calculated as shown in Fig. 8, where the range is ± 0.95 mm to prevent the mover from colliding the stator.

Fig. 8(a) shows the stable operation of the closed-loop system over the entire range. This clearly demonstrates that the controller $C(s)$ is able to regulate the nanopositioner whether it is in a stable or unstable state. However, the error $u - x$ varies between 80 nm and -117 nm for the 1.9 mm motion, which is handled in the next section.

In Fig. 8(c), the red dashed trend line captures the current's slope around the origin, which represents a case of linear nanopositioners for comparison. The current of the proposed nanopositioner follows the trend line around the origin. However, the nanopositioner requires less current than the trend line at positions far from the origin. Particularly at 0.95 mm the trend line indicates 4.74 A. In contrast, the proposed nanopositioner needs only 1.65 A, reducing the required current by 67 % in comparison to the trend line representing a linear positioner. Accordingly, positioning near the stroke ends requires less voltage and power than the point around ± 0.7 mm (Fig. 8(b)). Overall, the results clearly demonstrate the benefits of the nanopositioner that takes advantage of the system integration to utilize the nonlinearities for long-range and energy-efficient positioning.

D. Triangular motion

For accurate large scanning motion, a 1 Hz triangular wave of $\pm 800\,\mu$m is used as r, including the first 11 harmonics ($q_r = 11$) to prevent the saturation of the amplifier. The highest harmonics of the modeling-free IIC is tuned to $q = 100$ to sufficiently compensate for the nonlinearities. The results are shown in Fig. 9(a)-(c). At the 0th iteration in Fig. 9(a), the nanopositioner controlled only by the feedback controller results in a large tracking error $e = r - x$ of 4120 nm_{rms}, since the Type 1 system is unable to track r's ramp parts that are 3.2 mm/s. This error quickly converges. At the 15th iteration, the modeling-free IIC decreases the error by a factor of 396 to 10.4 nm_{rms}, demonstrating its effectiveness to compensate for the nonlinearities. Fig. 9(b)(c) show the signals in the time

Post-print version of the article: S. Ito, S. Troppmair, B. Lindner, F. Cigarini, and G. Schitter, "Long-Range Fast Nanopositioner Using Nonlinearities of Hybrid Reluctance Actuator for Energy Efficiency," *IEEE Transactions on Industrial Electronics*, vol. 66 (4), pp. 3051-3059, 2019. DOI: 10.1109/TIE.2018.2842735

This article has been accepted for publication in a future issue of this journal, but has not been fully edited. Content may change prior to final publication. Citation information: DOI 10.1109/TIE.2018.2842735, IEEE Transactions on Industrial Electronics

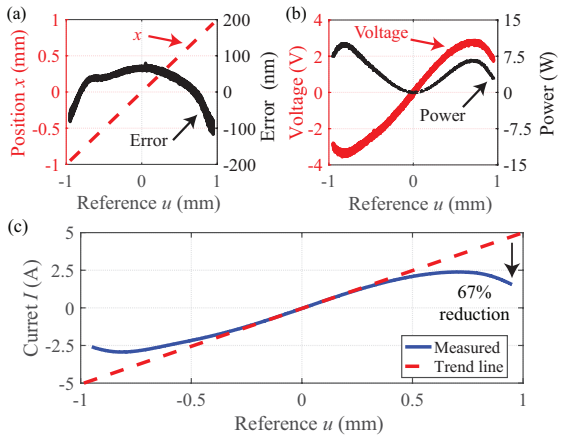

Fig. 8. Experimental results when the nanopositioner tracks a ramp reference u with a velocity of about 40 μm/s in a range of $\pm$0.95 mm: (a) measured mover position x and error, (b) voltage over the coils and power consumed by the nanopositioner, and (c) coil current and its trend line at the origin.

domain at the 15th iteration. It can be seen that the error is within $\pm$40 nm.

Dependent on applications, short-stroke scanning is required at a high frequency, as well [2]. To demonstrate the performance with such motion, a 100 Hz triangular wave of $\pm$5 μm is used near the stroke end (800 μm), including the first 11 harmonics. As shown in Fig. 9(a), the modeling-free IIC with $q = 17$ decreases the error e from 913 $\mathrm{nm_{rms}}$ at the 0th iteration to 10.0 $_{\mathrm{rms}}$ at the 15th iteration by a factor of 91. The results at the 15th iteration are shown in Fig. 9(d)(e), where the peak-to-peak error is within $\pm$25 nm. During the scanning, the coil voltage varies between 0.16 V and 4.30 V, and the current I varies between 1.93 A and 2.10 A, which are sufficiently smaller than the amplifier's maximum output voltage and current. This is because their DC components are reduced by the nanopositioner's nonlinearities, such that a small current and voltage enable high-speed scanning even near the stroke ends. In other words, the proposed nanopositioner is versatile, playing a role of both long-stroke and high-speed scanners.

Overall, the experimental results clearly demonstrate that the integrated nonlinearities can realize the energy efficient nanopositioner where the advanced motion control enables high-precision motion over a long range.

VII. Conclusion and Future Work

This paper proposes a flexure-guided nanopositioner with nonlinearities to decrease the current required for positioning. The model based analysis and FEA of a hybrid reluctance actuator selected for this purpose reveal that the position-dependent force can be regarded as negative stiffness canceling the flexure stiffness for the current reduction. For further reduction, the negative stiffness and the motor constant increase toward the stroke ends, however, causing a stability problem. This is solved by robust feedback control that is able to regulate the nanopositioner even if it is at a stable or unstable

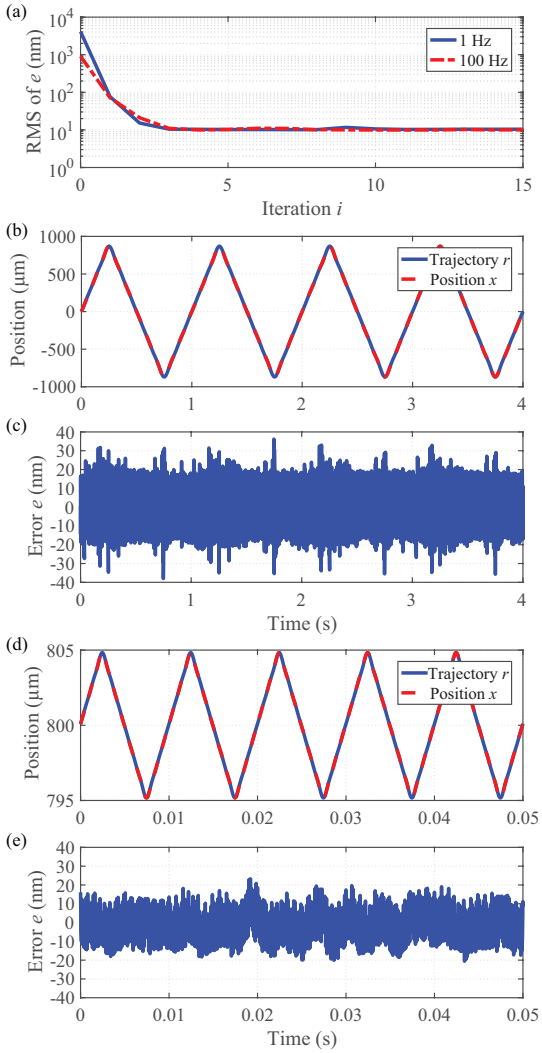

Fig. 9. Measured triangular motion using modeling-free IIC: (a) learning transient, (b)(c) 1 Hz triangular motion of $\pm$800 μm, and (d)(e) 100 Hz triangular motion of $\pm$5 μm.

position. Consequently, the nanopositioner is operated for the entire motion range of about $\pm$1 mm, achieving a positioning resolution of 2.48 $\mathrm{nm_{rms}}$ at a static point. The required current of the nonlinear nanopositioner is experimentally evaluated, and it is reduced by 64 % in comparison with a linearly designed case. The influence of the nonlinearities on the scanning motion is successfully compensated by modeling-free IIC, reducing the tracking error by a factor of 396. Consequently, the proposed nanopositioner achieves a tracking error of 10 $\mathrm{nm_{rms}}$ for a triangular scanning signal of 1.6 mm at 1 Hz, as well as for a triangular scanning of 10 μm at 100 Hz. Future work includes to develop a 2D nanopositioner based on hybrid reluctance actuators to enable a variety of motion trajectories for AFM and additive manufacturing.

Post-print version of the article: S. Ito, S. Troppmair, B. Lindner, F. Cigarini, and G. Schitter, "Long-Range Fast Nanopositioner Using Nonlinearities of Hybrid Reluctance Actuator for Energy Efficiency," *IEEE Transactions on Industrial Electronics*, vol. 66 (4), pp. 3051-3059, 2019. DOI: 10.1109/TIE.2018.2842735

This article has been accepted for publication in a future issue of this journal, but has not been fully edited. Content may change prior to final publication. Citation information: DOI 10.1109/TIE.2018.2842735, IEEE Transactions on Industrial Electronics

References

[1] M. Malinauskas, M. Farsari, A. Piskarskas, and S. Juodkazis, "Ultrafast laser nanostructuring of photopolymers: A decade of advances," *Physics Reports*, vol. 533, DOI 10.1016/j.physrep.2013.07.005, no. 1, pp. 1–31, 2013.

[2] P. Eaton and P. West, *Atomic Force Microscopy*. Oxford University Press, 2010.

[3] R. Saathof, M. Thier, R. Hainisch, and G. Schitter, "Integrated system and control design of a one DoF nano-metrology platform," *Mechatronics*, vol. 47, DOI 10.1016/j.mechatronics.2017.08.013, pp. 88 – 96, 2017.

[4] Y. K. Yong, S. O. R. Moheimani, B. J. Kenton, and K. K. Leang, "Invited review article: High-speed flexure-guided nanopositioning: Mechanical design and control issues," *Review of Scientific Instruments*, vol. 83, DOI 10.1063/1.4765048, no. 12, pp. –, 2012.

[5] G. Schitter, K. J. Astrom, B. E. DeMartini, P. J. Thurner, K. L. Turner, and P. K. Hansma, "Design and modeling of a high-speed afm-scanner," *IEEE Transactions on Control Systems Technology*, vol. 15, DOI 10.1109/TCST.2007.902953, no. 5, pp. 906–915, Sep. 2007.

[6] A. Bazaei, Y. K. Yong, and S. O. R. Moheimani, "Combining spiral scanning and internal model control for sequential AFM imaging at video rate," *IEEE/ASME Transactions on Mechatronics*, vol. 22, DOI 10.1109/TMECH.2016.2574892, no. 1, pp. 371–380, Feb. 2017.

[7] A. J. Fleming, "Nanopositioning system with force feedback for high-performance tracking and vibration control," *IEEE/ASME Transactions on Mechatronics*, vol. 15, DOI 10.1109/TMECH.2009.2028422, no. 3, pp. 433–447, Jun. 2010.

[8] B. J. Kenton and K. K. Leang, "Design and control of a three-axis serial-kinematic high-bandwidth nanopositioner," *IEEE/ASME Transactions on Mechatronics*, vol. 17, DOI 10.1109/TMECH.2011.2105499, no. 2, pp. 356–369, Apr. 2012.

[9] C. Yang, C. Li, and J. Zhao, "A nonlinear charge controller with tunable precision for highly linear operation of piezoelectric stack actuators," *IEEE Transactions on Industrial Electronics*, vol. PP, DOI 10.1109/TIE.2017.2698398, no. 99, pp. 1–1, 2017.

[10] R. Munnig Schmidt, G. Schitter, A. Rankers, and J. van Eijk, *The Design of High Performance Mechatronics*, 2nd ed. Delft University Press, 2014.

[11] S. Ito and G. Schitter, "Comparison and classification of high-precision actuators based on stiffness influencing vibration isolation," *IEEE/ASME Transactions on Mechatronics*, vol. 21, DOI 10.1109/TMECH.2015.2478658, no. 2, pp. 1169–1178, Apr. 2016.

[12] G. Parmar, K. Barton, and S. Awtar, "Large dynamic range nanopositioning using iterative learning control," *Precision Engineering*, vol. 38, DOI 10.1016/j.precisioneng.2013.07.003, no. 1, pp. 48–56, 2014.

[13] S. Ito, S. Unger, and G. Schitter, "Vibration isolator carrying atomic force microscope's head," *Mechatronics*, vol. 44, DOI 10.1016/j.mechatronics.2017.04.008, pp. 32–41, 2017.

[14] S. Ito, F. Cigarini, S. Unger, and G. Schitter, "Flexure design for precision positioning using low-stiffness actuators," in *7th IFAC Symposium on Mechatronic Systems (IFAC-PapersOnLine)*, vol. 49, DOI 10.1016/j.ifacol.2016.10.548, no. 21, pp. 200–205, 2016.

[15] P. Wang and Q. Xu, "Design of a flexure-based XY precision positioning stage with constant force output," in *Annual Conference of the IEEE Industrial Electronics Society*, DOI 10.1109/IECON.2016.7793662, pp. 524–529, Oct. 2016.

[16] T. Tuma, W. Haeberle, H. Rothuizen, J. Lygeros, A. Pantazi, and A. Sebastian, "Dual-stage nanopositioning for high-speed scanning probe microscopy," *IEEE/ASME Transactions on Mechatronics*, vol. 19, DOI 10.1109/TMECH.2013.2266481, no. 3, pp. 1035–1045, Jun. 2014.

[17] J. W. Wu, K. C. Huang, M. L. Chiang, M. Y. Chen, and L. C. Fu, "Modeling and controller design of a precision hybrid scanner for application in large measurement-range atomic force microscopy," *IEEE Transactions on Industrial Electronics*, vol. 61, DOI 10.1109/TIE.2013.2279352, no. 7, pp. 3704–3712, Jul. 2014.

[18] S. J. Schroeck, W. C. Messner, and R. J. McNab, "On compensator design for linear time-invariant dual-input single-output systems," *IEEE/ASME Transactions on Mechatronics*, vol. 6, DOI 10.1109/3516.914391, no. 1, pp. 50–57, Mar. 2001.

[19] B. J. Kenton, A. J. Fleming, and K. K. Leang, "Compact ultra-fast vertical nanopositioner for improving scanning probe microscope scan speed," *Review of Scientific Instruments*, vol. 82, DOI 10.1063/1.3664613, no. 12, p. 123703, 2011.

[20] H. Butler, "Position control in lithographic equipment," *IEEE Control Systems Magazine*, vol. 31, DOI 10.1109/MCS.2011.941882, no. 5, pp. 28 –47, 2011.

[21] S. Ito, J. Steininger, and G. Schitter, "Low-stiffness dual stage actuator for long rage positioning with nanometer resolution," *Mechatronics*, vol. 29, DOI 10.1016/j.mechatronics.2015.05.007, pp. 46–56, 2015.

[22] Q. Xu, "Continuous integral terminal third-order sliding mode motion control for piezoelectric nanopositioning system," *IEEE/ASME Transactions on Mechatronics*, vol. 22, DOI 10.1109/TMECH.2017.2701417, no. 4, pp. 1828–1838, Aug. 2017.

[23] X. Chen, C. Y. Su, Z. Li, and F. Yang, "Design of implementable adaptive control for micro/nano positioning system driven by piezoelectric actuator," *IEEE Transactions on Industrial Electronics*, vol. 63, DOI 10.1109/TIE.2016.2573270, no. 10, pp. 6471–6481, Oct. 2016.

[24] Y. Li and J. Bechhoefer, "Model-free iterative control of repetitive dynamics for high-speed scanning in atomic force microscopy," *Review of Scientific Instruments*, vol. 80, DOI 10.1063/1.3065093, no. 1, p. 013702, 2009.

[25] X. Lu, "Electromagnetically-driven ultra-fast tool servos for diamond turning," Ph.D. dissertation, Massachusetts Institute of Technology, 2005.

[26] D. J. Kluk, M. T. Boulet, and D. L. Trumper, "A high-bandwidth, high-precision, two-axis steering mirror with moving iron actuator," *Mechatronics*, vol. 22, DOI 10.1016/j.mechatronics.2012.01.008, no. 3, pp. 257–270, 2012.

[27] E. Csencsics, J. Schlarp, and G. Schitter, "Bandwidth extension of hybrid-reluctance-force-based tip/tilt system by reduction of eddy currents," in *International Conference on Advanced Intelligent Mechatronics*, DOI 10.1109/AIM.2017.8014176, pp. 1167–1172, Jul. 2017.

[28] D. Wu, X. Xie, and S. Zhou, "Design of a normal stress electromagnetic fast linear actuator," *IEEE Transactions on Magnetics*, vol. 46, DOI 10.1109/TMAG.2009.2036606, no. 4, pp. 1007–1014, Apr. 2010.

[29] M. K. Kazimierczuk, *High-Frequency Magnetic Components*, 2nd ed. Wiley, 2013.

[30] J. Van de Vegte, *Feedback Control Systems*, 3rd ed. Prentice Hall, 1994.

[31] Z. Wang and Q. Zou, "A modeling-free differential-inversion-based iterative control approach to simultaneous hysteresis-dynamics compensation," in *American Control Conference*, DOI 10.1109/ACC.2015.7171882, pp. 3558–3563, Jul. 2015.

[32] S. Ito, H. W. Yoo, and G. Schitter, "Comparison of modeling-free learning control algorithms for galvanometer scanner's periodic motion," in *IEEE International Conference on Advanced Intelligent Mechatronics*, DOI 10.1109/AIM.2017.8014207, pp. 1357–1362, Jul. 2017.

[33] M. Hehn and R. D'Andrea, "A frequency domain iterative learning algorithm for high-performance, periodic quadrocopter maneuvers," *Mechatronics*, vol. 24, DOI 10.1016/j.mechatronics.2014.09.013, no. 8, pp. 954 – 965, 2014.

[34] S. Tien, Q. Zou, and S. Devasia, "Iterative control of dynamics-coupling-caused errors in piezoscanners during high-speed AFM operation," *IEEE Transactions on Control Systems Technology*, vol. 13, DOI 10.1109/TCST.2005.854334, no. 6, pp. 921–931, Nov. 2005.

Shingo Ito received the MASc in Mechanical and Industrial Engineering from the University of Toronto, Canada, in 2007 and the PhD in Electrical Engineering from TU Wien, Vienna, Austria in 2015. From 2007 to 2010, he served as an engineer in the field of motion control at Yaskawa Electric Corporation, Japan.

He is currently a postdoctoral researcher at the Automation and Control Institute (ACIN), TU Wien. His research interest includes design and control of high-precision mechatronic systems for production, inspection and automation.

Post-print version of the article: S. Ito, S. Troppmair, B. Lindner, F. Cigarini, and G. Schitter, "Long-Range Fast Nanopositioner Using Nonlinearities of Hybrid Reluctance Actuator for Energy Efficiency," *IEEE Transactions on Industrial Electronics*, vol. 66 (4), pp. 3051-3059, 2019. DOI: 10.1109/TIE.2018.2842735

This article has been accepted for publication in a future issue of this journal, but has not been fully edited. Content may change prior to final publication. Citation information: DOI 10.1109/TIE.2018.2842735, IEEE Transactions on Industrial Electronics

Stefan Troppmair received the MSc in Automation Technology in 2017 from TU Wien, Vienna Austria. His research for the Master's degree focused on the design and control of high-precision actuators at the Automation and Control Institute (ACIN), TU Wien. Currently he serves as a software development engineer at Bosch Engineering GmbH, Vienna Austria, developing motor control units for combustion and hybrid cars.

Bernhard Lindner received the MSc in Automation Technology in 2018 from TU Wien, Vienna Austria. His research for the Master degree focused on high-precision actuators and their applications at the Automation and Control Institute (ACIN), TU Wien. Currently he serves as a researcher and developer of length and angle measurement systems at Flux GmbH (Braunau am Inn, Austria).

Francesco Cigarini is a PhD student at the Automation and Control Institute (ACIN) of TU Wien, Vienna, Austria. He received the MSc degree in mechatronic engineering from the University of Modena and Reggio Emilia, Reggio Emilia, Italy (2012). His research interest includes the design of mechatronic systems, inline metrology systems and multiphysics FEM analysis of electro-mechanical systems.

Georg Schitter (SM'11) is Professor for Advanced Mechatronic Systems at the Automation and Control Institute (ACIN) of TU Wien. He received an MSc in Electrical Engineering from TU Graz, Austria (2000) and an MSc and PhD degree from ETH Zurich, Switzerland (2004).

His primary research interests are on high-performance mechatronic systems, particularly for applications in the high-tech industry, scientific instrumentation, and mechatronic imaging systems, such as AFM, scanning laser and LIDAR systems, telescope systems, adaptive optics, and lithography systems for semiconductor industry.

He received the IFAC Mechatronics best paper award (2008-2011) and 2013 IFAC Mechatronics Young Researcher Award, and served as an Associate Editor for IFAC Mechatronics, Control Engineering Practice, and for the IEEE-Transactions on Mechatronics.

Post-print version of the article: S. Ito, S. Troppmair, B. Lindner, F. Cigarini, and G. Schitter, "Long-Range Fast Nanopositioner Using Nonlinearities of Hybrid Reluctance Actuator for Energy Efficiency," *IEEE Transactions on Industrial Electronics*, vol. 66 (4), pp. 3051-3059, 2019. DOI: 10.1109/TIE.2018.2842735